Digital Signal Processing 19 (2009) 780–792

Contents lists available at ScienceDirect

Digital Signal Processing

www.elsevier.com/locate/dsp

Superresolution algorithms for spatial extended scattering centers

Felix Totir [a], Emanuel Radoi [b,*]

[a] Military Technical Academy, 81-83 G. Cosbuc Avenue, 050141 Bucharest, Romania
[b] Université Européenne de Bretagne, CNRS, UMR 3192 Lab-STICC, ISSTB, 6 avenue Victor Le Gorgeu, CS 93837, 29238 Brest cedex 3, France

ARTICLE INFO

Article history:
Available online 16 April 2009

Keywords:
Superresolution radar imagery
MUSIC
ESPRIT
Extended scattering centers

ABSTRACT

Scattering centers model (SCM) is usually considered for modeling target backscattered signal in high-resolution radar. In this case the impulse response of each scattering center is represented by a time-delayed Dirac pulse. Some of most popular superresolution imagery techniques, such as MUSIC or ESPRIT, are well-matched to this model. Under this hypothesis, they outperform Fourier-based techniques in terms of both spatial and dynamic resolutions. However, the behavior of real-world targets is often very different from that of the SCM. Indeed, their reflectivity function is not confined just to several perfectly localized scattering centers, but it can be rather approximated by a set of scattering regions having different spatial extent. SCM becomes then inappropriate and the superresolution methods may provide unexpected results. Furthermore, the amplitude information is difficult to interpret in this case. In this paper we propose an extension of two superresolution methods, MUSIC and ESPRIT, to cope with extended scattering centers (ESC). According to this model, the impulse response of an ESC is not a Dirac pulse, but a window of finite support. Besides the position, the size (spatial extent) of this window is also recovered. This additional information about the target structure can be used for increasing ATR (automatic target recognition) accuracy and robustness.

1. Introduction

Radar targets are usually modeled by a set of perfectly localized scattering centers when a broadband transmitted signal is used [7]. They account for isotropic, non-dispersive and strong reflections on the target surface. Although these hypotheses are only approximately true in practice, the SCM simplicity makes it the most common model in ISAR imagery.

ISAR images, in either 1D (range profiles) [17], 2D (ISAR images) [21] or 3D representations, provide valuable signatures for ATR [5]. Excepting the tomographic methods [8,25], most of imagery techniques are essentially spectral analysis methods, such as Fourier transform, linear prediction or superresolution algorithms [9,24], etc.

In the last-mentioned algorithm class, MUSIC (multiple signal classification) [4] and ESPRIT (estimation of signal parameters by rotational invariance techniques) [22] are the most popular methods. Both of them are subspace decomposition techniques, taking advantage of the autocorrelation matrix eigenstructure. Its eigenvectors span the observation space into two orthogonal subspaces, usually called signal and the noise subspaces. The positions of the target scattering centers are estimated either using a variable mode vector which is continuously projected onto the noise subspace (MUSIC algorithm), or as solutions of a matrix eigenanalysis problem (ESPRIT algorithm).

Different extensions of the two algorithms have been proposed: computationally less intensive root-MUSIC [13], 2D [16], 3D [26] or multidimensional [19] versions. We reported some imagery results on both synthetic and measured data in [18].

* Corresponding author. Fax: +33 298 01 63 95.
E-mail address: emanuel.radoi@univ-brest.fr (E. Radoi).

1051-2004/$ – see front matter
doi:10.1016/j.dsp.2009.04.002

An important shortcoming of these methods is that they are model-dependant. Their performances may drop significantly if the echo signal does not match the SCM assumption. This may happen, for instance, whenever the scattering structures are not perfectly localized, as in the case of dihedral angles [11]. The impulse response of this kind of structure can be represented as the convolution of a Dirac pulse, giving its spatial position, and of a finite length window, giving its spatial extension. The aspect-dependent nature of these physical structures is apparent for large angular intervals only, and is ignored here. In this paper we will call these scattering structures Extended Scattering Centers (ESCs). Note that a standard scattering center is just a special case of an ESC.

Standard MUSIC and ESPRIT methods either skip ESCs or misinterpret them as a set of scattering centers. Hence, the true nature of the scattering process is hidden in this case. Detecting ESCs in a proper manner allows recovering the structural information, which is claimed to be the most useful in ATR [23].

The problem of non point-like scattering centers has been already addressed in [3], in a SAR context. The proposed approach, called HDVI (high-definition vector imaging), combines Capon's maximum likelihood method and a modified MUSIC algorithm in order to take into account this kind of scattering centers and to enable feature detection.

In this paper we extend both MUSIC and ESPRIT algorithms to cope with ESC modeled targets in an ISAR context. Unlike the standard versions of these algorithms, the proposed e-MUSIC and e-ESPRIT methods are shown to properly detect ESCs and to provide their position and spatial extent.

The paper is organized as follows. The ESC target model is first defined in Section 2. The two proposed algorithms, e-MUSIC and e-ESPRIT, are then introduced in Section 3. They are compared to standard MUSIC and ESPRIT methods in Section 4. Finally, some limitations of the new algorithms are discussed in Section 5, while the conclusion is drawn in Section 6.

2. ESC-based target model

ESCs are modeled using time-delayed finite-support signals. Let $h(t)$ denote the temporal shape of the picked window (e.g. rectangular or Gaussian). It is normalized, so that:

$$\int_{-\infty}^{\infty} h(t)\,dt = 1. \tag{1}$$

Let Q be the total ESC number of the target. The qth ESC is then defined by its amplitude γ_q, delay τ_q and spatial extent (width) factor $\mu_q \geqslant 0$ (the index q varies from 0 to $Q-1$). Thus, its impulse response can be written as:

$$\chi_q(t;\gamma_q,\tau_q,\mu_q) = \gamma_q h_q(t;\tau_q,\mu_q) \tag{2}$$

where $h_q(t;\tau_q,\mu_q) = \frac{1}{\mu_q} h(\frac{t-\tau_q}{\mu_q})$ also meets (1).

In practice, Q is unknown. For standard SC, a number of techniques may be used for estimating it: AIC [1], MDL [2], Gerschgörin [10] or RAD [20]. Presumably, these methods could be generalized in order to estimate the number of ESC, too. However, more pragmatic approaches could be used. For example, [3] simply uses the rank of the covariance matrix (Eq. (10)) as an estimate for the number of ESC. Our experiments have shown that unlike ESPRIT algorithm, MUSIC is robust to the overestimation of Q. This different behavior is due to the vector subspace used by each of the two methods: the noise subspace for MUSIC and, respectively, the signal subspace for ESPRIT.

A comparison between the impulse responses of an ideal SC and of an ESC is shown in Fig. 1. Obviously, the shape of the window $h(t)$ is target dependant and, for real targets, it is *a priori* unknown. For now, some mathematical properties will be assumed for $h(t)$ and, in a later stage, we will consider a less restricted case.

For a given aspect, ESC echoes sum up and the target impulse response becomes:

$$\chi(t) = \sum_{q=0}^{Q-1} \chi_q(t;\gamma_q,\tau_q,\mu_q). \tag{3}$$

Consequently, the ideal transfer function is

$$X(f) = \sum_{q=0}^{Q-1} \gamma_q \exp(-j2\pi f\tau_q) H(f\mu_q). \tag{4}$$

In the above equation, $H(\cdot)$ is the Fourier transform of $h(\cdot)$. Obviously, $H(f\mu_q)$ represents the Fourier transform of $h(t/\mu_q)/\mu_q$.

The delay corresponding to the target rotation center is supposed to be canceled by phase compensation [6]. Then, if (u_{0q}, v_{0q}) are the qth ESC coordinates (see Fig. 2), its delay can be expressed as:

$$\tau_q = \frac{2d_q}{c} = \frac{2(u_{0q}\cos\beta + v_{0q}\sin\beta)}{c} \tag{5}$$

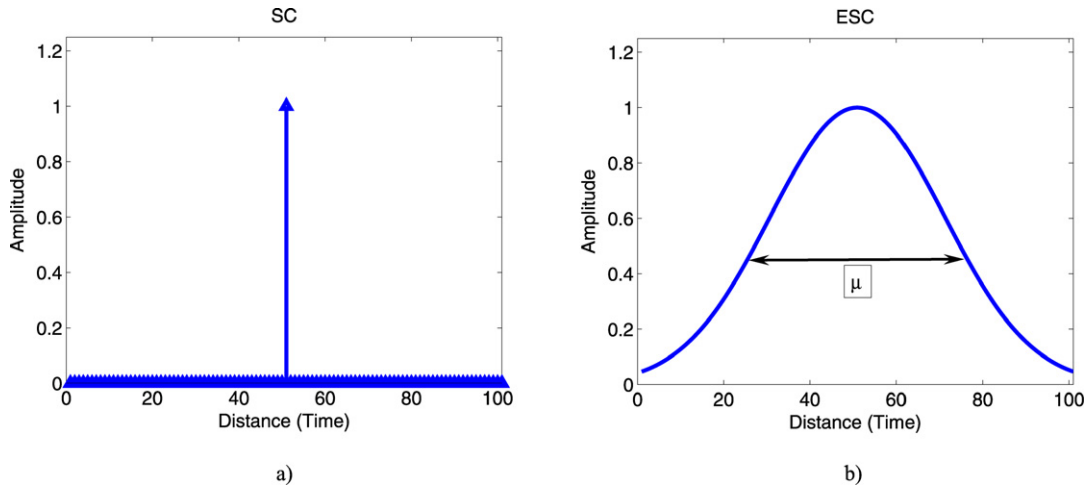

Fig. 1. Impulse response of an ideal SC (a) and of an extended SC, when a Gaussian window $h(t)$ is considered (b).

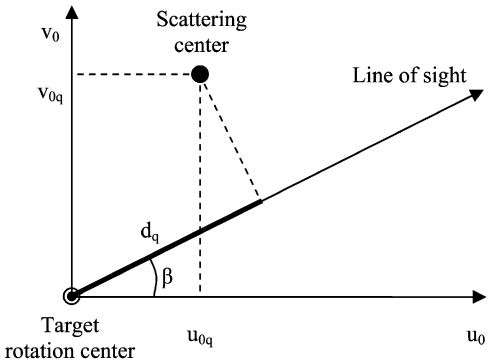

Fig. 2. Scattering center projection on the line of sight for a given target aspect.

where c is the speed of light, β is the target aspect and d_q is the distance between the target rotation center and the projection of the qth scattering center on the line of sight.

Replacing Eq. (5) in Eq. (4) results in:

$$X(f,\beta)=\sum_{q=1}^{Q}\gamma_q\exp\left(-j\frac{4\pi f}{c}(u_{0q}\cos\beta+v_{0q}\sin\beta)\right)H(f\mu_q). \tag{6}$$

The values of $X(f,\beta)$ for a discrete set of frequencies f_m $(m=0,\ldots,M-1)$ and aspect angles β_n $(n=0,\ldots,N-1)$ form the (2D) *complex signature* of the target. We will further consider its matrix form, with columnwise and linewise variations for frequency and aspect angle, respectively.

The reconstruction of 2D ISAR images usually involves a polar reformatting step [18]. Interpolation is used to obtain the target complex signature Y for a grid of uniformly spaced spatial frequencies $f^{(x)}=f\cos\beta$ and $f^{(y)}=f\sin\beta$ (where β is the target aspect angle). Conversely, the physical frequencies corresponding to the points of this grid are given by $f=\sqrt{(f^{(x)})^2+(f^{(y)})^2}$. Eq. (6) becomes then:

$$X\left(f^{(x)},f^{(y)}\right)=\sum_{q=1}^{Q}\gamma_q\exp\left(-j\frac{4\pi}{c}\left(u_{0q}f^{(x)}+v_{0q}f^{(y)}\right)\right)H\left(\sqrt{\left(f^{(x)}\right)^2+\left(f^{(y)}\right)^2}\mu_q\right). \tag{7}$$

It is straightforward to extend the presented 2D model to the 3D framework or to obtain the 1D model as a particular case.

3. e-MUSIC and e-ESPRIT algorithms

3.1. e-MUSIC algorithm

We will introduce this algorithm using a similar approach to that we have already considered in [18]. Thus, in a noisy environment, the complex signature equation for the 1D target model can be expressed in the following form:

$$\begin{bmatrix} Y(f_0) \\ Y(f_1) \\ \vdots \\ Y(f_{M-1}) \end{bmatrix} = \begin{bmatrix} X(f_0) \\ X(f_1) \\ \vdots \\ X(f_{M-1}) \end{bmatrix} + \begin{bmatrix} w_0 \\ w_1 \\ \dots \\ w_{M-1} \end{bmatrix} = \mathbf{A} \begin{bmatrix} \gamma_0 \\ \gamma_1 \\ \dots \\ \gamma_{Q-1} \end{bmatrix} + \begin{bmatrix} w_0 \\ w_1 \\ \dots \\ w_{M-1} \end{bmatrix} \tag{8}$$

where

$$\mathbf{A} = \begin{bmatrix} e^{-j2\pi f_0 \tau_0} H(\mu_0 f_0) & e^{-j2\pi f_0 \tau_1} H(\mu_1 f_0) & \dots & e^{-j2\pi f_0 \tau_{Q-1}} H(\mu_{Q-1} f_0) \\ e^{-j2\pi f_1 \tau_0} H(\mu_0 f_1) & e^{-j2\pi f_1 \tau_1} H(\mu_1 f_1) & \dots & e^{-j2\pi f_1 \tau_{Q-1}} H(\mu_{Q-1} f_1) \\ \vdots & \vdots & \vdots & \vdots \\ e^{-j2\pi f_{M-1} \tau_0} H(\mu_0 f_{M-1}) & e^{-j2\pi f_{M-1} \tau_1} H(\mu_1 f_{M-1}) & \dots & e^{-j2\pi f_{M-1} \tau_{Q-1}} H(\mu_{Q-1} f_{M-1}) \end{bmatrix} \tag{9}$$

and w_m $(m = 0, \dots, M-1)$ are (white) noise samples.

Compared to standard MUSIC algorithm, the structure of the matrix $\mathbf{A}$ is modified by the factors $\{H(\mu_q f_m)\}_{q=0,\dots,Q-1,\ m=0,\dots,M-1}$. The estimation of the autocorrelation matrix of the complex signature is based on the spatial smoothing procedure [13].

Under the white noise assumption, the autocorrelation matrix satisfies:

$$\mathbf{R}_{YY} = \mathbf{R}_{XX} + \sigma^2 \mathbf{I}_M \tag{10}$$

where σ^2 is the noise power, and

$$\mathbf{R}_{XX} = [r_{m_1 m_2}]_{m_1, m_2 = 0,\dots,M-1} \tag{11}$$

with

$$r_{m_1 m_2} = \sum_{q=0}^{Q-1} |\gamma_q^2| e^{j2\pi (f_{m_2} - f_{m_1}) \tau_q} H(\mu_q f_{m_1}) H^*(\mu_q f_{m_2}). \tag{12}$$

The eigenvectors of the autocorrelation matrix corresponding to its greatest Q eigenvalues span the same vector space as the columns of matrix $\mathbf{A}$ (the signal subspace), while the others span the noise subspace. Let us form a new matrix $\mathbf{V_n}$ by taking the noise subspace eigenvectors as columns. Similarly to the standard MUSIC algorithm, e-MUSIC estimate is then given by

$$P_{\text{e-MUSIC 1D}}(\tau, \mu) = \frac{1}{\tilde{\boldsymbol{a}}(\tau, \mu)^H \mathbf{V_n} \mathbf{V_n}^H \tilde{\boldsymbol{a}}(\tau, \mu)} \tag{13}$$

where

$$\tilde{\boldsymbol{a}}(\tau, \mu) = \begin{bmatrix} \exp(-j2\pi f_0 \tau) H(\mu f_0) & \dots & \exp(-j2\pi f_{p-1} \tau) H(\mu f_{p-1}) \end{bmatrix}^T \tag{14}$$

is the mode vector, which has a similar form to the columns of the matrix $\mathbf{A}$, τ_q and μ_q being replaced by τ and μ respectively.

$\{f_k\}_{k=0\dots p-1}$ are the frequency steps used for the data acquisition process, while $p > Q$ is the spatial smoothing window length. It is chosen between $M/2$ and $2M/3$ [18] in order to ensure a good trade-off between the spatial resolution and the covariance matrix condition number (or scattering center decorrelation). This choice differs from the one considered in [15], which relies on some experiments with the MSTAR dataset [14]. In this case p is chosen around $M/3$, in order to obtain twice as many subbands (windows) as the dimension of the covariance matrix.

It is important to note that the e-MUSIC algorithm introduces a new search dimension along the μ-axis. Consequently, the reconstructed range profile will be represented as a 2D intensity map, its maxima coding both time delays and spatial extent factors associated to the target ESCs. The main drawback is an increasing computation time because of the new added search dimension. Consequently, for more complex ESC model, parameterized by more than two variables, the computational burden becomes a significant issue for e-MUSIC algorithm implementation.

e-MUSIC algorithm improves the information about the target scattering properties in two ways:

- all the scattering centers have been properly detected (there is no missing SC or outliers);
- two parameters are associated to each detected scattering center (spatial extent and position).

Consider now the 2D case. The equivalent matrix equation has the following form:

$$\mathbf{Y} = \mathbf{X} + \mathbf{w} = \mathbf{A} \begin{bmatrix} \gamma_0 \\ \gamma_1 \\ \vdots \\ \gamma_{Q-1} \end{bmatrix} + \mathbf{w} \tag{15}$$

where $\mathbf{X}$ is the columnwise concatenation of the target complex signature and $\mathbf{w}$ is the vector of noise samples.

The matrix $\mathbf{A}$ has the following form:

$$\mathbf{A} = [\, \boldsymbol{a}_0 \quad \ldots \quad \boldsymbol{a}_{Q-1} \,] \tag{16}$$

with

$$\boldsymbol{a}_q = \boldsymbol{a}_q(\tau_{x_q}, \tau_{y_q}, \mu_q) = \begin{bmatrix} e^{-j2\pi f_0^{(x)} \tau_{x_q}} e^{-j2\pi f_0^{(y)} \tau_{y_q}} H\left(\mu_q \sqrt{\left(f_0^{(x)}\right)^2 + \left(f_0^{(y)}\right)^2}\right) \\ e^{-j2\pi f_1^{(x)} \tau_{x_q}} e^{-j2\pi f_0^{(y)} \tau_{y_q}} H\left(\mu_q \sqrt{\left(f_1^{(x)}\right)^2 + \left(f_0^{(y)}\right)^2}\right) \\ \vdots \\ e^{-j2\pi f_{p_1-1}^{(x)} \tau_{x_q}} e^{-j2\pi f_{p_2-1}^{(y)} \tau_{y_q}} H\left(\mu_q \sqrt{\left(f_{p_1-1}^{(x)}\right)^2 + \left(f_{p_2-1}^{(y)}\right)^2}\right) \end{bmatrix}. \tag{17}$$

Finally, the mode vector is similar to the columns of the matrix $\mathbf{A}$:

$$\tilde{\boldsymbol{a}}(\tau_x, \tau_y, \mu) = \begin{bmatrix} e^{-j2\pi f_0^{(x)} \tau_x} e^{-j2\pi f_0^{(y)} \tau_y} H\left(\mu \sqrt{\left(f_0^{(x)}\right)^2 + \left(f_0^{(y)}\right)^2}\right) \\ e^{-j2\pi f_1^{(x)} \tau_x} e^{-j2\pi f_0^{(y)} \tau_y} H\left(\mu \sqrt{\left(f_1^{(x)}\right)^2 + \left(f_0^{(y)}\right)^2}\right) \\ \vdots \\ e^{-j2\pi f_{p_1-1}^{(x)} \tau_x} e^{-j2\pi f_{p_2-1}^{(y)} \tau_y} H\left(\mu \sqrt{\left(f_{p_1-1}^{(x)}\right)^2 + \left(f_{p_2-1}^{(y)}\right)^2}\right) \end{bmatrix} \tag{18}$$

and e-MUSIC 2D estimate becomes:

$$P_{\text{e-MUSIC 2D}}(x, y, \mu) = \frac{1}{\tilde{\boldsymbol{a}}(\tau_x, \tau_y, \mu)^H \mathbf{V_n} \mathbf{V_n}^H \tilde{\boldsymbol{a}}(\tau_x, \tau_y, \mu)}. \tag{19}$$

Similarly, in the 3D case, the mode vector has the following expression:

$$\tilde{\boldsymbol{a}}(x, y, z, \mu) = \begin{bmatrix} e^{-j2\pi f_0^{(x)} \tau_x} e^{-j2\pi f_0^{(y)} \tau_y} e^{-j2\pi f_0^{(z)} \tau_z} H\left(\mu \sqrt{\left(f_0^{(x)}\right)^2 + \left(f_0^{(y)}\right)^2 + \left(f_0^{(z)}\right)^2}\right) \\ e^{-j2\pi f_1^{(x)} \tau_x} e^{-j2\pi f_0^{(y)} \tau_y} e^{-j2\pi f_0^{(z)} \tau_z} H\left(\mu \sqrt{\left(f_1^{(x)}\right)^2 + \left(f_0^{(y)}\right)^2 + \left(f_0^{(z)}\right)^2}\right) \\ \vdots \\ e^{-j2\pi f_{p_1-1}^{(x)} \tau_x} e^{-j2\pi f_{p_2-1}^{(y)} \tau_y} e^{-j2\pi f_{p_3-1}^{(z)} \tau_z} H\left(\mu \sqrt{\left(f_{p_1-1}^{(x)}\right)^2 + \left(f_{p_2-1}^{(y)}\right)^2 + \left(f_{p_3-1}^{(z)}\right)^2}\right) \end{bmatrix} \tag{20}$$

where $f^{(x)}$, $f^{(y)}$ and $f^{(z)}$ are spatial frequencies obtained by applying the polar formatting algorithm (PFA) [27] in the 3D case. e-MUSIC 3D estimate takes then the following form:

$$P_{\text{e-MUSIC 3D}}(\tau_x, \tau_y, \tau_z, \mu) = \frac{1}{\tilde{\boldsymbol{a}}(\tau_x, \tau_y, \tau_z, \mu)^H \mathbf{V_n} \mathbf{V_n}^H \tilde{\boldsymbol{a}}(\tau_x, \tau_y, \tau_z, \mu)}. \tag{21}$$

3.2. e-ESPRIT algorithm

Let us now assume that the frequencies used to acquire the target complex signature form an arithmetic progression with the common difference δ_f:

$$f_{m+1} = f_m + \delta_f, \quad m = 0 \ldots M-2. \tag{22}$$

Let us also consider the following constraint for the function $H(f)$:

$$H(\omega_1 + \omega_2) = K \cdot H(\omega_1) H(\omega_2), \quad \forall \omega_1, \omega_2 \geqslant 0 \tag{23}$$

which, particularly, ensures that:

$$H(\mu f_m + \mu \delta_f) = K \cdot H(\mu f_m) H(\mu \delta_f), \quad m = 0 \ldots M-2 \tag{24}$$

with $C(\mu) = K \cdot H(\mu \delta_f)$ acting as a (m-independent) constant. This could be seen as an admissibility condition for the window function $h(t)$.

Table 1
1D target ESC parameters.

	ESC 1	ESC 2	ESC 3	ESC 4
Delay (norm.)	0.1	0.2	0.3	0.75
Width (norm.)	0.02	0.02	0.06	0.01
Energy	1	1	1	1

Then, the following equation holds:

$$\bar{\mathbf{A}} = \underline{\mathbf{A}}\boldsymbol{\Theta}, \tag{25}$$

where

$$\boldsymbol{\Theta} = \operatorname{diag}\big(C(\mu_0)\exp(-j2\pi\delta_f\tau_0) \quad \ldots \quad C(\mu_{Q-1})\exp(-j2\pi\delta_f\tau_{Q-1}) \big) \tag{26}$$

and $\bar{\mathbf{A}}$ and $\underline{\mathbf{A}}$ are obtained by dropping respectively the first and the last row of the matrix $\mathbf{A}$.

Further, we follow an ESPRIT-like approach [12]. The covariance matrix $\mathbf{R}_{YY}$ is estimated and its eigenvalues and eigenvectors are computed. Consider now the matrix $\mathbf{V}$, whose columns are the eigenvectors of $\mathbf{R}_{YY}$ spanning the signal subspace (i.e. the eigenvectors corresponding to the largest Q eigenvalues of $\mathbf{R}_{YY}$). Since the columns of the matrices $\mathbf{V}$ and $\mathbf{A}$ span the same vector space (specifically, the signal subspace) [12], these two matrices are equivalent, which results in:

$$\mathbf{AT} = \mathbf{V} \tag{27}$$

where $\mathbf{T}$ is an invertible transformation matrix.

Further, we introduce the matrices $\bar{\mathbf{V}}$ and $\underline{\mathbf{V}}$, obtained by dropping respectively the first and the last row of the matrix $\mathbf{V}$. Note that $\bar{\mathbf{V}} = \bar{\mathbf{A}}\mathbf{T}$ and $\underline{\mathbf{V}} = \underline{\mathbf{A}}\mathbf{T}$.

Making use of Eq. (26), we are now able to write:

$$(\underline{\mathbf{V}})^{\dagger}\bar{\mathbf{V}} = \mathbf{T}^{-1}\boldsymbol{\Theta}\mathbf{T}, \tag{28}$$

where the † symbol stands for the pseudo-inverse operator.

Consequently, the eigenvalues of the matrix $\boldsymbol{\Theta}$ (which are exactly its diagonal elements) are also the eigenvalues of the matrix $(\underline{\mathbf{V}})^{\dagger}\bar{\mathbf{V}}$. Thus, by computing the eigenvalues of $(\underline{\mathbf{V}})^{\dagger}\bar{\mathbf{V}}$, one retrieves in fact the diagonal elements of $\boldsymbol{\Theta}$, whose phases code the ESCs delays (positions), while their magnitudes give the corresponding spatial extent factors (see Eq. (26)).

Possible examples for $H(f)$, which meet the admissibility constraint are $H(f) = \exp(\alpha f)$ or $H(f) = \exp(\alpha|f|)$, $\alpha \in \mathbb{C}$ (with $K = 1$). Note that the case $C(\mu) = K \cdot H(\mu\delta_f) \equiv 1$ leads to the standard ESPRIT algorithm.

It is straightforward to extend the e-ESPRIT algorithm presented above to the 2D and 3D cases, using a very similar approach to that already used in [18].

4. Simulation results

Let us consider the target defined by the 4 ESCs having the parameters given in Table 1. They have the same energy (integral of squared impulse response), which is normalized to be 1. Hence, the corresponding amplitudes vary with the associated width factor. The target impulse response, obtained using Eq. (3) for $Q = 4$, is shown in Fig. 3a. Let us also assume that the ESCs impulse responses are modeled via the following function:

$$h(t) = \frac{1}{\pi(t^2+1)} \xrightarrow{\text{Fourier Transform}} H(f) = e^{-2\pi|f|}. \tag{29}$$

This function has been chosen to satisfy the admissibility condition (24), which is required when using the e-ESPRIT algorithm.

Note that for $\mu \to 0$, $\frac{1}{\mu}h(\frac{t-\tau}{\mu}) \to \delta(t-\tau)$ and $H(\mu f) \to 1$, so that the ESC model becomes a standard SCM one.

With this input data, the 1D target complex signature has been generated using Eq. (4). A number of 20 frequency bins have been considered, the frequency step being normalized to 1. Accordingly, the 1D target complex signature is a complex vector of length 20.

The range profile obtained by inverse Fourier transform of the target complex signature is shown in Fig. 3b. It approximates the target impulse response reasonably well. The same number of points (201) have been used to plot both range profiles in Figs. 3a and 3b. It is worth noting that, given enough bandwidth, all visible ESC are well resolved in position, but the one with largest spatial extent (the third) is hidden because of the poor dynamic resolution.

Likewise, standard MUSIC 1D algorithm fails in discriminating all ESCs, as shown in Fig. 3c, because of the spatial extent of the third scattering center. MUSIC estimate was computed and plotted using the same number of 201 bins.

However, e-MUSIC 1D algorithm correctly separates all the 4 ESCs, with no visible secondary lobes (see Fig. 4b). e-MUSIC 1D algorithm returns a 2D intensity map (Fig. 4a), whose maxima allows simultaneous reading the time delay (horizontal axis) and the spatial extent (vertical axis) corresponding to each ESC (theoretically with infinite accuracy, by actually limited

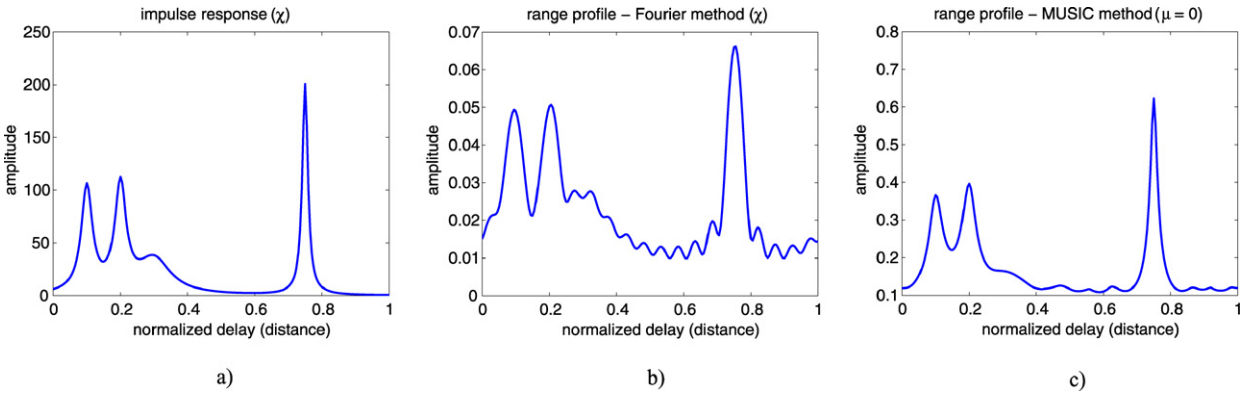

Fig. 3. 1D target impulse response (a), Fourier 1D (b) and MUSIC 1D (c) reconstructed range profiles.

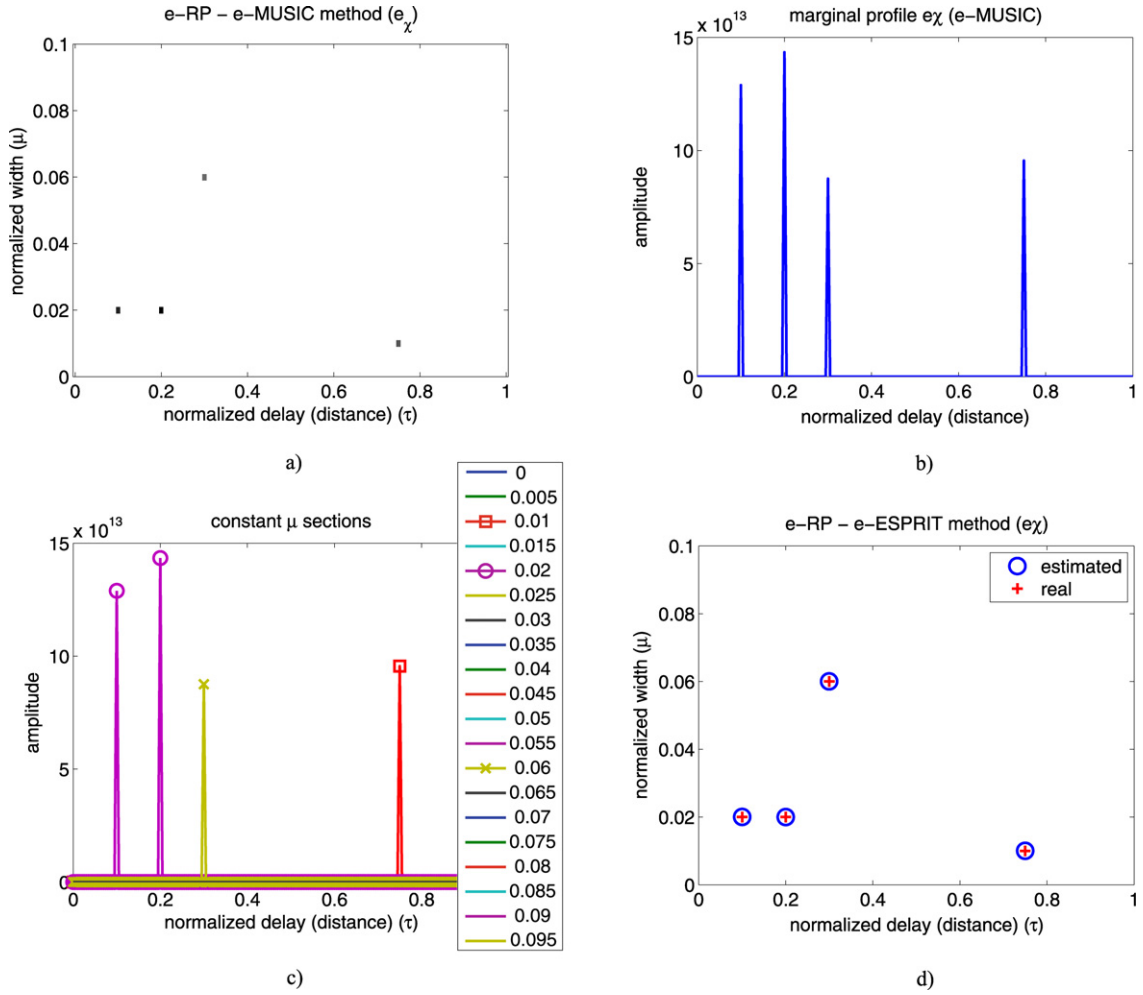

Fig. 4. e-RP reconstructed using e-MUSIC 1D (a), its marginal (b), some constant spatial extent (width is symbol/color-coded) sections (c) and e-RP reconstructed using e-ESPRIT 1D (d).

by the computer representation precision and by the number of points used to compute the estimate). Such representation, combining ESCs delays and spatial extent information, will be referred to as extended range profile (e-RP).

Sections of constant spatial extent (here from 0 to 0.1) which are nothing more than plots of the lines of the e-RP in Fig. 4a, are shown in Fig. 4c. Only three of them (highlighted using symbols, which code the underlying width too) are non-zero, corresponding to the following width factors: 0.01, 0.02 and 0.06.

Table 2
2D target ESCs parameters.

	ESC 1	ESC 2	ESC 3	ESC 4	ESC 5	ESC 6	ESC 7
τ_x (norm.)	0	0.2	−0.2	0.2	−0.2	0.2	−0.2
τ_y (norm.)	−0.4	−0.2	−0.2	0	0	0.2	0.2
Width (norm.)	0.01	0.05	0.05	0.02	0.02	0.03	0.03
Energy	1	1	1	1	1	1	1

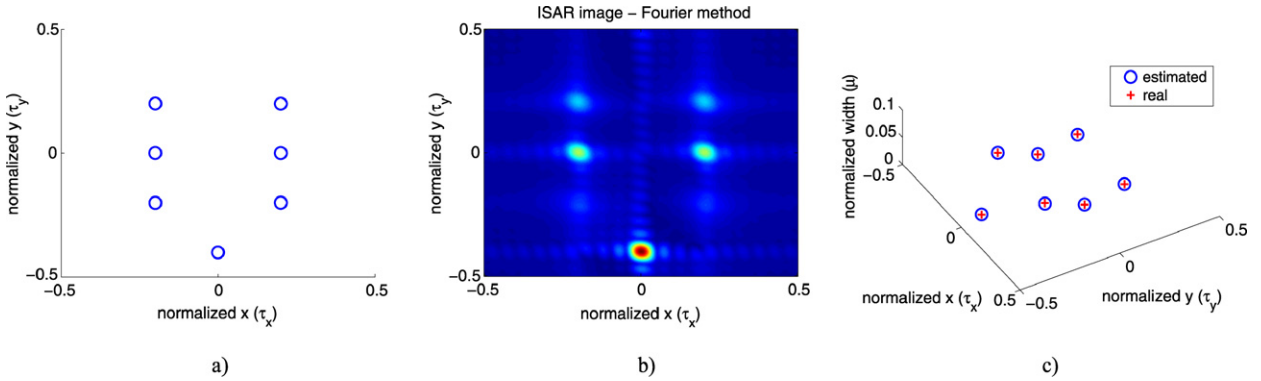

Fig. 5. Positions of the ESCs defining the 2D target (a), its Fourier 2D-reconstructed ISAR image (b) and e-RP reconstructed using e-ESPRIT 2D (c).

It is possible to exploit this information in different ways. For example, one can simply average the e-RP with respect to the spatial extent (Fig. 4b). This kind of representation, which preserves the delay information only and averages or ignores the widths, will be termed as marginal (it may be defined for either e-MUSIC or e-ESPRIT). It allows us to quickly identify the number of detected e-SC and their locations and, thus, it may be regarded as the counterpart of the standard MUSIC estimate and compared to it. Note that the delay (location) information is not obvious in the case of standard MUSIC estimate (see Fig. 3c).

Alternatively, the model equation (3) may be used to synthesize the target range profile (impulse response) from the ESCs' delays and widths, as recovered by e-MUSIC or e-ESPRIT. In this case, the obtained range profile (not shown) is very similar to the ideal one, depicted in Fig. 3a.

The discrete e-RP reconstructed using e-ESPRIT 1D is shown in Fig. 4d.

During our experiments, we noticed that only forward averaging (non-symmetric) estimate of the autocorrelation matrix was able to provide expected results. This confirms Benitz's remarks on the estimation of the sample covariance matrix [3], prohibiting the use of forward–backward averaging technique in covariance matrix estimation when target's phase response is not symmetric (such as the azimutal-flash model presented therein). Specifically, for the different sub-looks involved in averaged autocorrelation matrix estimation, the shape of ESC response would not be preserved when backward looks are considered.

Hence, the forward–backward averaging (symmetric) estimate of the autocorrelation matrix tends to destroy the spatial extension information associated with a given ESC. It is felt by the authors that this can be grasped easier if one considers the delay and width estimation dual problem, i.e. the problem of both frequency and bandwidth estimation. Thus, the duals of finite width, time-delayed ESC are finite bandwidth, frequency-centered signals (let say, chirps). Forward–backward averaging estimation of the autocorrelation matrix will mix the direct and the reversed chirps. Thus, the (mean) frequency information (analogous to the ESC location) is somewhat preserved, while the bandwidth information (analogous to the ESC width) is destroyed, since direct and reverse chirps are mixed.

Next, we consider a 2D-distributed target, whose ESCs parameters are given in Table 2. ESCs positions are also shown in Fig. 5a.

Integrating 20 range profiles via 2D Fourier transform leads to the ISAR image depicted in Fig. 5b. In this image, the ESCs with large spatial extent are less visible, while their dimensions are not apparent. However, e-ESPRIT 2D algorithm successfully identifies ESCs delays and associated spatial extent coefficients, as shown in Fig. 5c.

A study of additive white Gaussian noise influence has been also performed and the results are shown in Fig. 6. Target complex signature has been generated and corrupted with complex white Gaussian noise, whose power is function of SNR (defined as the ratio between the target complex signature and noise powers). For each SNR, the range profile of the 1D target defined by Table 1 is reconstructed using Fourier 1D, e-MUSIC 1D and e-ESPRIT 1D algorithms and compared with the ideal one (target impulse response depicted in Fig. 3a). The reconstruction accuracy is measured via the mean squared error (MSE) and correlation coefficient. To obtain the former, the ideal and each of the synthesized range profiles (obtained from e-MUSIC and e-ESPRIT through Eq. (3)) were considered as vectors over a number of computing points, and the norm of their difference has been taken, then divided by the number of computing points. The correlation coefficients represent the covariance between the ideal and each of the synthesized range profiles (seen as vectors), further divided by the product of

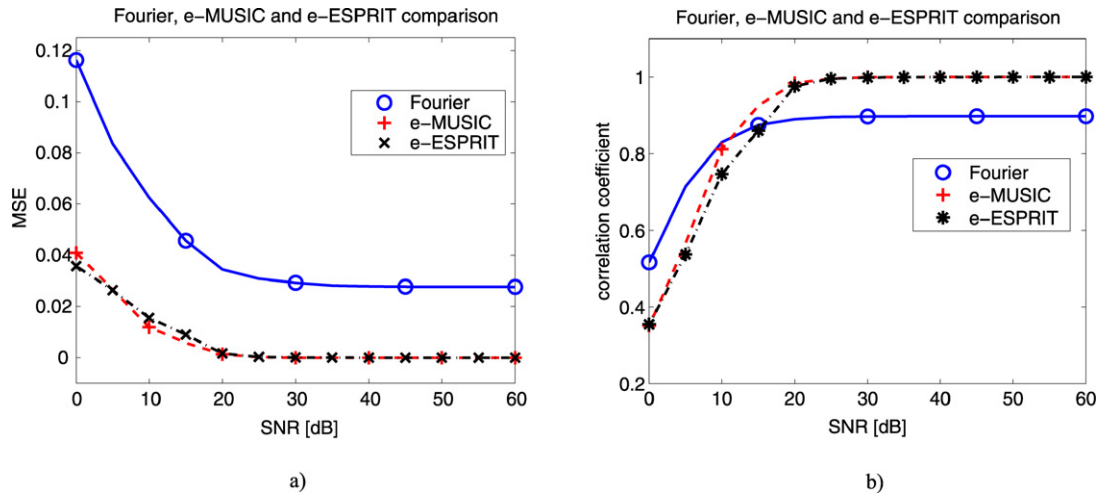

Fig. 6. MSE (a) and correlation coefficient (b) variations as functions of SNR.

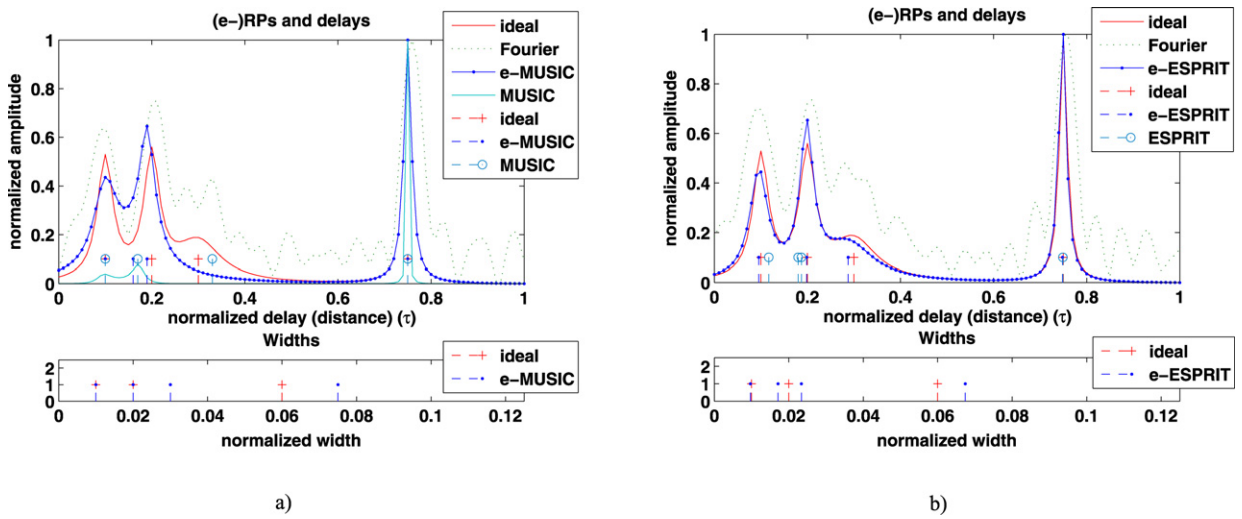

Fig. 7. Ideal RP and RPs reconstructed using Fourier, e-MUSIC, MUSIC and e-ESPRIT techniques, along with the ideal and estimated ESC locations and widths (see text for explanations).

their norms. The curves displayed in Fig. 6 were obtained by averaging 250 independently noisy realizations for each SNR level.

These results show that the Fourier 1D reconstruction method is penalized by its sidelobes and the bias of its maxima locations. Hence, the corresponding MSE is important, even for high SNR.

For lower SNRs, the correlation coefficient drops faster for e-MUSIC and e-ESPRIT, because of their higher sensitivity to parameter estimation errors. Consequently, the reconstructed range profile shape deteriorates rapidly for SNRs inferior to 10–15 dB. However, for high SNR, e-RPs are better suited for ATR since they also provide a meaningful structural description of the target.

Samples of the reconstructed range profiles are presented in Fig. 7, along with extracted information about the target. The two realizations are independent, but they share the same SNR (15 dB). The corresponding range profiles (or target impulse responses) have been either estimated directly, as the inverse Fourier of target complex signature, or synthesized (via Eq. (3)) from the estimated delays and widths of the ESCs recovered by e-MUSIC (Fig. 7a) and e-ESPRIT (Fig. 7b) algorithms, respectively.

In each upper subfigure, the positions of sticks below the curves are the normalized ideal and real locations of ESCs, as recovered by the corresponding e-MUSIC and MUSIC (Fig. 7a) or e-ESPRIT and ESPRIT (Fig. 7b) algorithms. The lower subfigures show the ideal and the estimated ESC widths, either by e-MUSIC (Fig. 7a) or e-ESPRIT (Fig. 7b) methods. Fig. 7a also presents the MUSIC reconstructed RP, from which the corresponding ESC locations are estimated.

Fig. 7 confirms that e-MUSIC and e-ESPRIT techniques perform better than their standard counterparts. Furthermore, some ESCs widths are also well estimated. It is important to note that this improvement is not limited to the perfect

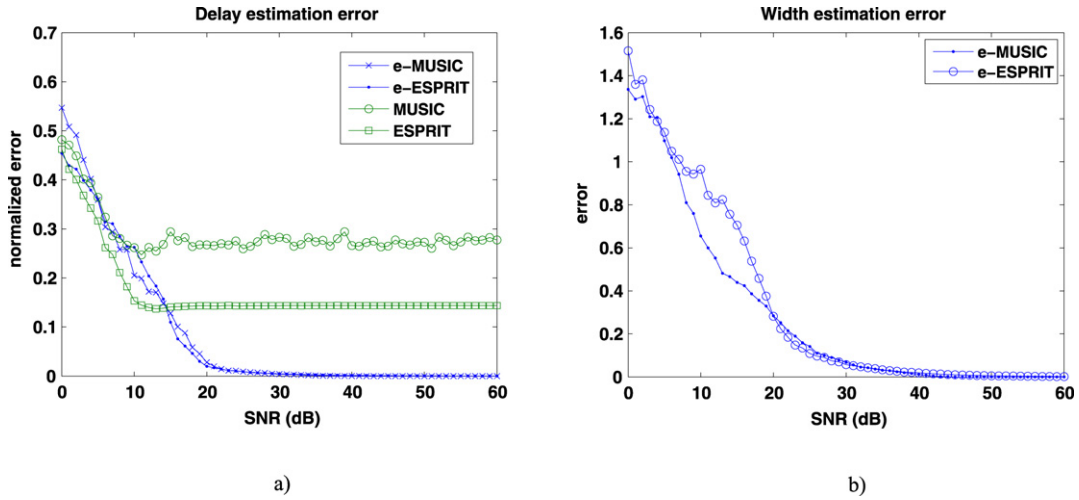

Fig. 8. Delay (a) and width (b) estimation errors for extended and standard MUSIC and ESPRIT.

reconstruction of the target impulse response. Indeed, the structural decomposition (locations and widths) of the target impulse response should be far more valuable in the event of target identification.

The information extracted by e-MUSIC and e-ESPRIT during the simulations above may be quickly analyzed using the delay (location) and width estimation error, as presented in Fig. 8.

Note that the behavior of e-MUSIC and e-ESPRIT is quite similar and, at high SNRs, both achieve almost perfect estimation of ESCs parameters. However, ESPRIT and MUSIC fail to achieve the same results, even asymptotically, because their underlying assumed model (zero-width SCs) is not appropriate.

At low SNR, the location estimation error converges for the 4 methods shown in Fig. 8. Since the location error is normalized, this simply shows that the estimation becomes almost unreliable for all methods. However, at high SNR, extended versions of both superresolution algorithms show a clear advantage: not only they better estimate ESC locations, but they provide the width information, too.

5. e-MUSIC and e-ESPRIT limitations

The performance of the methods introduced above is limited in real world applications, since the windowing function $h(t)$ is not known, so that the admissibility condition (23) cannot be checked. These reasons lead to difficulties when using the presented algorithms.

One obvious question is what happens when the "real" windowing function $h(t)$, let us rename it $h_1(t)$, is unknown. In this case, an approximation $h_2(t)$ can be considered to reconstruct (less accurately) the target model.

Let us consider $h_1(t) = e^{-t^2}$, which leads to $H_1(f) = \sqrt{\pi} e^{-\pi^2 f^2}$, and $h_2(t)$ given by Eq. (29). The widths and amplitudes (energies) of the ESCs are the ones in Table 1.

In this case, the mode vector used by e-MUSIC (1D) algorithm no more matches the columns of matrix **A** (since the former assumes $h_2(t)$-modeled ESCs, while the latter is looking for $h_1(t)$-modeled ones). As a result, the localization of the ESC will be less accurate. Similarly, in the case of e-ESPRIT (1D) algorithm, Eqs. (23) and (25) hold no more (i.e. $h(t)$ does not respect the admissibility condition), while in Eq. (26) the function linking diagonal elements amplitudes with coefficients μ_q will be erroneously assumed as depending on $H_2(f)$ instead of $H_1(f)$.

The reconstruction of the e-RPs confirms that the localization of the ESCs in this case, as shown in Fig. 9, is less accurate. The sub-optimal character of the problem is mostly visible in the width dimension, since the vector space decomposition and, particularly, columns of matrix **A** become non-orthogonal mainly because of the width-dependent $H(\mu_q f_m)$ factors (see Eq. (9)). Specifically, Fig. 9b illustrates the case when the e-SC are modeled by a width-function which do not respect the admissibility condition in (24). As shown, e-ESPRIT algorithm still reveals an useful, although somewhat perturbed, information.

However, even if the information concerning the width factors (μ_q) of the ESCs is corrupted, the reconstructed e-RPs successfully detect all of them at the right positions (unlike MUSIC 1D algorithm, as shown in Fig. 3c). Furthermore, although the 2D representation is less accurate along the vertical axis, the relative widths of the identified ESCs are somehow preserved, which still constitutes a valuable structural information.

So, compared to the standard MUSIC and ESPRIT reconstructed profiles, the improvement is still noticeable. Indeed, Fig. 10 shows that the RP obtained using the delay information provided by e-ESPRIT algorithm is more accurate than the RP reconstructed using the ESPRIT algorithm.

Similar conclusions may be drawn from the results depicted in Fig. 11 for MUSIC and e-MUSIC reconstructed RP. Unlike the former, who misses one SC, the latter successfully identifies all the SCs and accurately estimates their positions (delays).

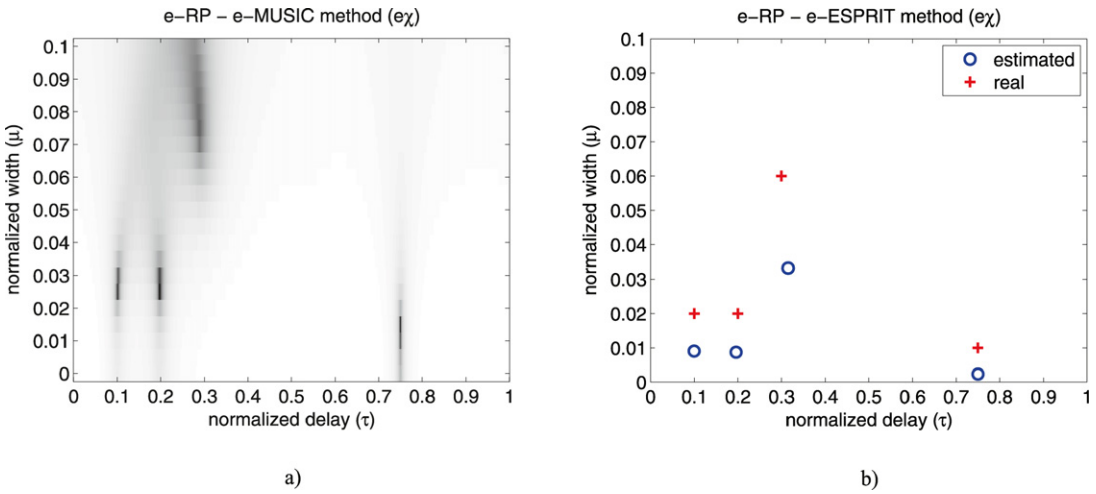

Fig. 9. e-RPs reconstructed using e-MUSIC 1D (a) and e-ESPRIT 1D (b) algorithms, when the windowing function is unknown.

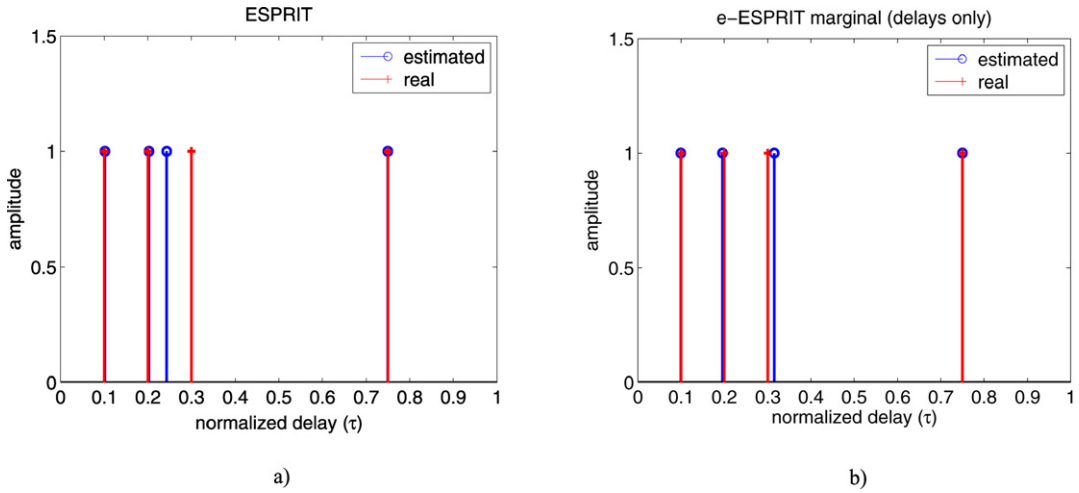

Fig. 10. Target estimated RP reconstructed using standard ESPRIT (a) or obtained using delay information provided by e-ESPRIT algorithm (b).

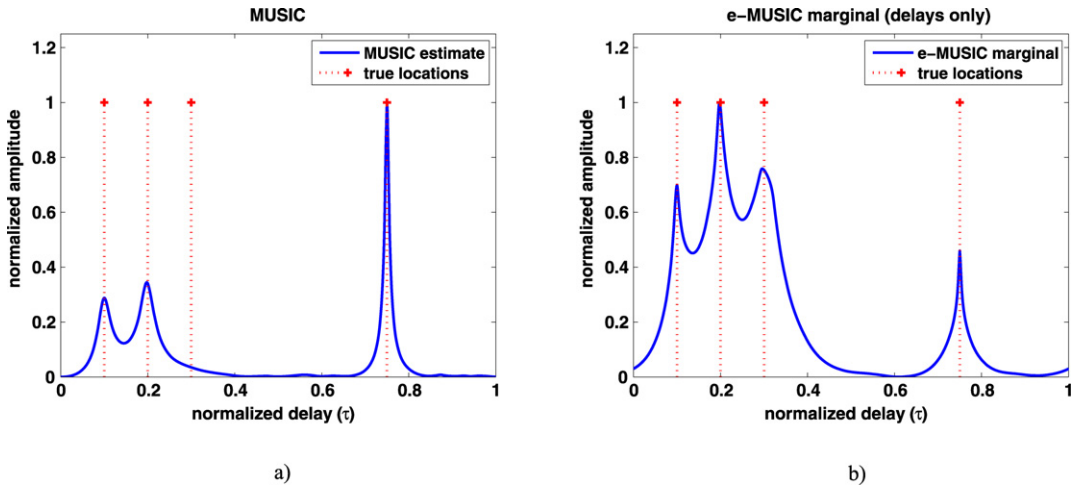

Fig. 11. Target estimated RP reconstructed using standard MUSIC (a) or obtained as a marginal of e-RP provided by the e-MUSIC algorithm (b).

6. Conclusion

In this paper we have shown that the performances of radar imagery algorithms MUSIC and ESPRIT are model-dependant. Indeed, they are adapted to Dirac-modeled scattering centers. However, real targets are often characterized by a contiguous scattered energy density function. In this case, standard versions of MUSIC and ESPRIT provide unexpected results, which are difficult to interpret. Hence, we have proposed extended forms for the two algorithms, in order to cope with this kind of targets. While still referred, the assumed target model is more general than for standard versions of MUSIC and ESPRIT. Some numerical results demonstrate the new method capabilities in terms of resolution and robustness. Our future work will focus on the estimation of the windowing function for real targets in order to increase the representation accuracy of the *e-RP* along the width axis.

Acknowledgments

This work is supported by NATO Grant EAP.RIG.982933. We would like to thank the anonymous referees for their careful reading and valuable comments and suggestions.

References

[1] H. Akaike, A new look at the statistical model identification, IEEE Trans. Automat. Control 19 (6) (1974) 716–723.
[2] A. Barron, J. Rissanen, B. Yu, The minimum description length principle in coding and modeling, IEEE Trans. Inform. Theory 44 (6) (1998) 2743–2760.
[3] G.R. Benitz, High-definition vector imaging, MIT Lincoln Laboratory J. – Special Issue on Superresolution 10 (2) (1997) 147–170.
[4] G. Bienvenu, L. Kopp, Adaptivity to background noise spatial coherence for high resolution passive methods, in: Proceedings of International Conference on Acoustics, Speech and Signal Processing (ICASSP), vol. 5, Denver, April 1980, pp. 307–310.
[5] B. Borden, Mathematical problems in radar inverse scattering, Inverse Problems 18 (1) (2002).
[6] V.C. Chen, H. Ling, Time–Frequency Transforms for Radar Imaging and Signal Analysis, Artech House Publishers, London, 2002.
[7] T. Cooke, M. Martorella, B. Haywood, D. Gibbins, Use of 3D ship scatterer models from ISAR image sequences for target recognition, Digital Signal Process. 16 (5) (2006) 523–532.
[8] Y. Dai, K.M. Chen, P. Nyquist, Time-domain imaging of radar targets using algorithms for reconstruction from projections, IEEE Trans. Antennas and Propagation 45 (8) (1997) 1227–1235.
[9] I.J. Gupta, High-resolution radar imaging using 2-D linear prediction, IEEE Trans. Antennas and Propagation 42 (1) (1994) 31–37.
[10] A.S. Householder, The Theory of Matrices in Numerical Analysis, Dover Publications, New York, 1975.
[11] J. Li, P. Stoica, An adaptive filtering approach to spectral estimation and SAR imaging, IEEE Trans. Signal Process. 44 (6) (1996) 1469–1484.
[12] S. Marcos, J. Sanchez-Araujo, N. Bertaux, P. Larzabal, P. Forster, Les méthodes à haute résolution – traitement d'antenne et analyse spectrale, Hermès Science Publications, Paris, 1998.
[13] S.L. Marple, Digital Spectral Analysis: With Applications, Prentice Hall, Englewood Cliffs, NJ, 1987.
[14] Air Force Research Laboratory (Sensor Data Management System), Moving and Stationary Target Acquisition and Recognition, https://www.sdms.afrl.af.mil/datasets/mstar/.
[15] D. Nguyen, G. Benitz, J. Kay, B. Orchard, R. Whiting, Superresolution HRR ATR with high definition vector imaging, IEEE Trans. Aerosp. Electron. Syst. 37 (4) (2001) 1267–1286.
[16] J.W. Odendaal, E. Barnard, C.W.I. Pistorius, Two-dimensional superresolution radar imaging using the MUSIC algorithm, IEEE Trans. Antennas and Propagation 42 (10) (1994) 1386–1391.
[17] A. Quinquis, S. Demeter, E. Radoi, Enhancing the resolution of the radar target range profiles using a class of subspace eigenanalysis-based techniques, Digital Signal Process. 11 (4) (2001) 288–303.
[18] A. Quinquis, E. Radoi, F. Totir, Some radar imagery results using superresolution techniques, IEEE Trans. Antennas and Propagation 52 (5) (2004) 1230–1244.
[19] E. Radoi, A. Quinquis, F. Totir, Achieving superresolution by subspace eigenanalysis in multidimensional spaces, in: Proceedings of the 11th European Signal Processing Conference (EUSIPCO'2002), Toulouse, 03–06 September 2002.
[20] E. Radoi, A. Quinquis, A new method for estimating the number of harmonic components in noise with application in high-resolution radar, EURASIP J. Appl. Signal Process. 2004 (8) (2004) 1177–1188.
[21] F. Rice, T. Cooke, D. Gibbins, Model based ISAR ship classification, Digital Signal Process. 16 (5) (2006) 628–637.
[22] R. Roy, T. Kailath, ESPRIT – Estimation of signal parameters via rotational invariance techniques, IEEE Trans. Acoust. Speech Signal Process. 37 (7) (1989) 984–995.
[23] P.B. Silverstein, O.S. Sands, F.D. Garber, Radar target classification and interpretation by means of structural descriptions of backscatter signals, IEEE Aerosp. Electron. Syst. Mag. 6 (5) (1991) 3–7.
[24] S.D. Silverstein, M.D. Zoltowski, The mathematical basis for element and Fourier beam space MUSIC and root-MUSIC algorithms, Digital Signal Process. 1 (3) (1991) 161–175.
[25] L. Stankovic, I. Djurovic, T. Thayaparan, Separation of target rigid body and micro-Doppler effects in ISAR imaging, IEEE Trans. Aerosp. Electron. Syst. 42 (4) (2006) 1496–1506.
[26] P. Strobach, Total least squares phased averaging and 3-D ESPRIT for joint azimuth-elevation-carrier estimation, IEEE Trans. Signal Process. 49 (1) (2001) 54–62.
[27] D.R. Wehner, High Resolution Radar, second ed., Artech House Publishers, 1994.

Felix Totir received the B.S. degree in radar and guidance systems from the Military Technical Academy of Bucharest in 2002. In 2003 he received the M.S. degree, in telecommunications, and in 2006 the Ph.D. degree, in signal processing, both from the University of Brest. He is currently with the Military Technical Academy of Bucharest and conducts scientific projects for the Romanian MoD. He is interested in radar signal processing, automatic object recognition, time–frequency analysis, dynamical systems and cellular automata.

Emanuel Radoi was born in 1968. He graduated in radar systems at the Military Technical Academy of Bucharest, in 1992. In 1997 he received the M.S. degree, in electronic engineering, and in 1999 the Ph.D. degree, in signal processing, both from the University of

Brest. He is currently Professor of Signal Processing in the Electronics Department of the University of Brest. His main research interests include superresolution methods, radar imagery, NCTR and UWB signal processing. He co-authored 7 books and more than 75 journal and conference papers.